JMEPEG (2011) 20:1554–1562
DOI: 10.1007/s11665-011-9855-x

1059-9495/$19.00

Effects of SiC Particle Size and Process Parameters on the Microstructure and Hardness of AZ91/SiC Composite Layer Fabricated by FSP

P. Asadi, M.K. Besharati Givi, K. Abrinia, M. Taherishargh, and R. Salekrostam

(Submitted April 6, 2010; in revised form August 22, 2010)

In this study, friction stir processing (FSP) was employed to develop a composite layer on the surface of as-cast AZ91 magnesium alloy using SiC particles (5 μm and 30 nm). The effects of the rotational and traverse speeds and the FSP pass number on the microstructure and microhardness of the friction stir processed (FSPed) layer with and without SiC particles were investigated. Optical microscopy and scanning electron microscopy (SEM) were employed for microstructural analysis. FSP produces a homogeneous microstructure by eliminating the precipitates near the grain boundaries. The analyses showed that the effects of the rotational and traverse speeds on the microstructure of specimens produced without nano-sized SiC particles are considerable; however, they are negligible in the specimens with particles. While the second FSP pass enhances the microstructure and microhardness of the samples with SiC particles, it has no significant effect on such properties in the samples without SiC particles.

Keywords FSP, hardness, magnesium alloy, microstructure modification

1. Introduction

Nowadays, one of the biggest challenges in the transportation industry is finding ways to develop new structural materials with higher strength to weight ratios. Magnesium is the lightest structural metal which is 35% lighter than aluminium and 78% lighter than steel (Ref 1). However, its poor formability and ductility caused by hexagonal, close-packed crystal structure limit its use in some applications at room temperature (Ref 2, 3). The alloying of magnesium with some elements such as Al, Zn, Mn, and Ca is a conventional way to improve its properties (Ref 4). The successfully fabricated various nano-sized wires, powders, or tubes have made it possible to modify the structural and functional characteristics of the existing commercial materials (Ref 5). Among these, discontinuously reinforced metal matrix composites (MMCs) receive increasing attention because various types of reinforcement are available. Besides, there are successful manufacturing processes for producing MMCs which can be utilized to fabricate these MMCs (Ref 6). Some parameters which determine the properties of MMCs include the intrinsic properties of reinforcement and matrix, the shape, size, volume fraction, orientation, and distribution of the reinforcement phase (Ref 7).

Al- or Mg-based MMCs are fabricated by several methods including stir casting (Ref 4), ultrasonic cavitation (Ref 8), blend-press-sinter methodology (Ref 7), squeeze casting, and powder metallurgy (Ref 5). Recently, a new surface modification technique named friction stir processing (FSP) has been at the center of attention. FSP is a solid-state processing technique based on FSW principles, in which a rotating tool with a special design travels down the surfaces of metal plates. This is achieved by producing a highly plastically deformed zone through the associated stirring action. The final structure of the stirred zone (SZ) consists of fine and equiaxed grains, produced as a result of dynamic recrystallization (Ref 1-5).

The FSP has been basically considered as an advanced process for grain refinement techniques. It is also very attractive for fabricating composite (Ref 9, 10).

Lee et al. (Ref 9) produced AZ61Mg-based composites with nano-SiO2 particles and improved hardness and high strain rate superplasticity of the base material. Morisada et al. successfully dispersed Fullerene into A5083 by FSP and modified the hardness and grain size of the base alloy (Ref 11). They also fabricated MWCNTs/AZ31 surface composites by this process (Ref 10). Lee et al. incorporated nano-sized SiO_2 ceramic particles into the AZ61Mg alloy matrix via FSP and improved the mechanical and microstructural properties of this alloy (Ref 5). The authors, in line with these and other similar experiments, have produced AZ91/SiC composite via FSP in a previous study (Ref 12), but the effect of process parameters on the properties of fabricated composite is still in need of more investigations.

In this study, FSP was employed to fabricate composite and nanocomposite layers on the surface of as-cast AZ91 magnesium alloy using 5 μm and 30 nm SiC particles. Attempt has been made to investigate the effect of major FSP parameters (rotational speed, traverse speed, and pass number) and

P. Asadi, M.K. Besharati Givi, K. Abrinia, and **R. Salekrostam**, School of Mechanical Engineering, College of Engineering, University of Tehran, Tehran, Iran; and **M. Taherishargh**, School of Mining and Metallurgical Engineering, Amirkabir University of Technology, Hafez Street, P.O. Box 15875/4413, Tehran, Iran. Contact e-mails: mehdi.taheri.sh@gmail.com and mehdy_tahery@aut.ac.ir.

reinforcing particle size on the microstructure, grain size and microhardness of the developed surface.

2. Experimental Details

Commercially available SiC powders with average sizes of 5 μm and 30 nm and 99.8% purity were used as reinforcement particles with the volume fraction of 7.5% for each. The SiC particles were filled into a groove (0.8 mm × 1.2 mm) machined on the AZ91 as-cast plate with the thickness of 5 mm. The composition of AZ91 was (in wt.%): Al, 9.1; Zn, 0.68; Mn, 0.21; Si, 0.085; Cu, 0.0097; Ni, 0.001; Fe, 0.0029; and Mg, bal.

Two 2344 hot working steel tools are shown in Fig. 1. A pinless tool was employed to cover the top of the grooves after being filled with SiC particles to prevent the particles from scattering during FSP. Another tool was inserted into the prepared specimen by the first tool to carry out FSP. It had a square pin with dimensions of 3.5 mm × 3.5 mm and length of 2.5 mm. Both tools' shoulders were 15 mm in diameter. It should be noted that, the first tool had the constant rotational and traverse speeds of 710 rpm and 40 mm/min, respectively, in all the experiments. The rotational speed of the second tool was varied from 710 to 1400 rpm, and the traverse speeds varied from 12.5 to 63 mm/min. The FSP tool was rotated clockwise with the tilt angle of 3°.

For microstructural observations, the transverse sections of the specimens were prepared by standard metallographic techniques and etched with a solution of 5 mL acetic acid, 6 g picric acid, 10 mL water, 100 mL ethanol, 5 mL HCl, and 7 mL nitric acid for 1-2 s. The microstructural observations of the stirred zone (SZ) were carried out by optical microscopy and scanning electron microscopy (SEM). Energy dispersive spectroscopy (EDS) analysis was employed to obtain the composition of different regions of the specimens. Microhardness of the specimens was measured in points with 1-mm distance from the upper surface and 0.25-mm distance from one another in the cross section to acquire the microhardness profiles using a Vickers microhardness testing machine by applying a load of 200 g for 15 s.

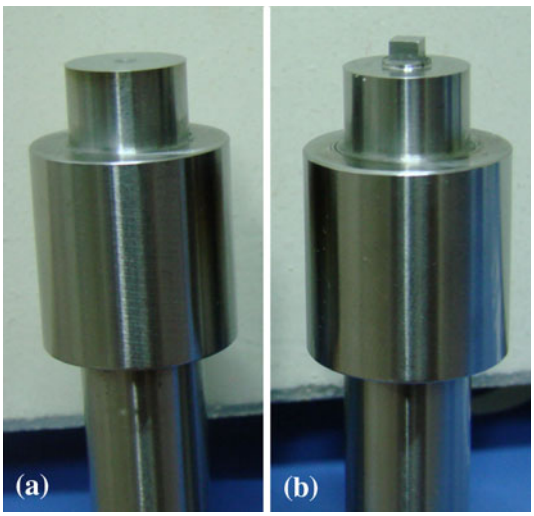

Fig. 1 (a) Tool without pin and (b) tool with square pin

3. Results and Discussion

The SZ dimensions were about 5 mm in width and 2.5 mm in depth, which were in the same range of rotating pin dimensions. Figure 2 presents the microstructure of FSPed as-cast AZ91 magnesium alloy with 5 μm SiC particles. Three distinct zones are clear in the figure: stirred zone, thermo-mechanically affected zone (TMAZ), and heat affected zone (HAZ). The basic microstructure of AZ91 magnesium alloy consists of primary α-phase in which aluminium rich β-phase ($Mg_{17}Al_{12}$) is precipitated along the grain boundaries (Ref 13). While the average grain size is about 150 μm in the base metal, it is about 10 μm in the SZ that is much finer. Homogenous microstructure, including very fine and equiaxed grains, was obtained via dynamic recrystallization. SEM micrograph of the SZ is shown in Fig. 3(a). EDS analysis carried out in the grain boundary as well as inside the grain (Fig. 3b, c) shows that the compositions of both are the same and β-phase did not precipitate at the grain boundaries. Therefore, FSP causes the whole dispersed β-phase network to dissolve into α-phase, and a uniform chemical composition is developed.

Grains in the TMAZ have a special orientation and are elongated in the boundary between the SZ and the base metal (Fig. 2). It seems that there is no recrystallization in the TMAZ because the received heat and the amount of deformation are too low (Ref 14). Grain size of SZ depends on FSP parameters which generate the heat and SiC particles which restrict the grain growth by pinning effect during recrystallization. The white particles in Fig. 3(a) are 5 μm SiC particles which were identified using the EDS composition analysis (Fig. 3d). Figure 3(a) illustrates that the grains are much finer in the

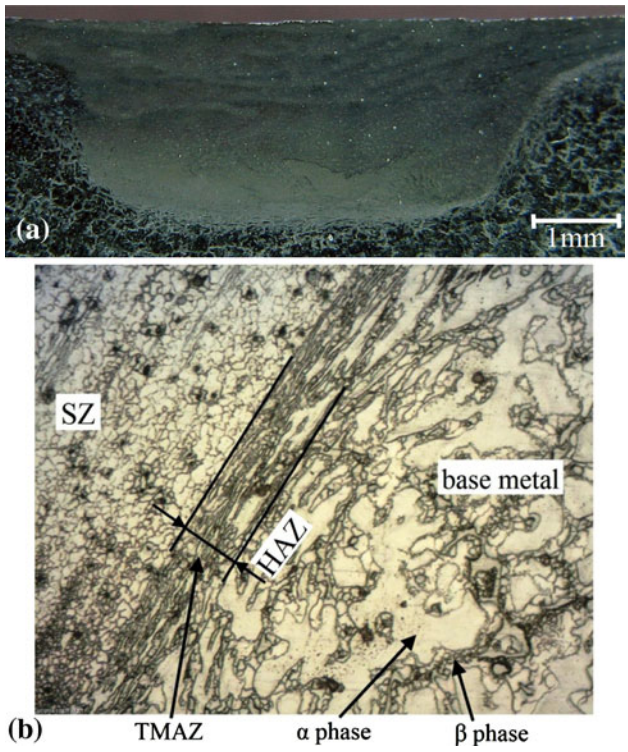

Fig. 2 (a) Macro image from cross section of the FSPed specimen, and (b) different zones of FSPed specimen. The rotational and traverse speeds were 900 rpm and 63 mm/min, respectively

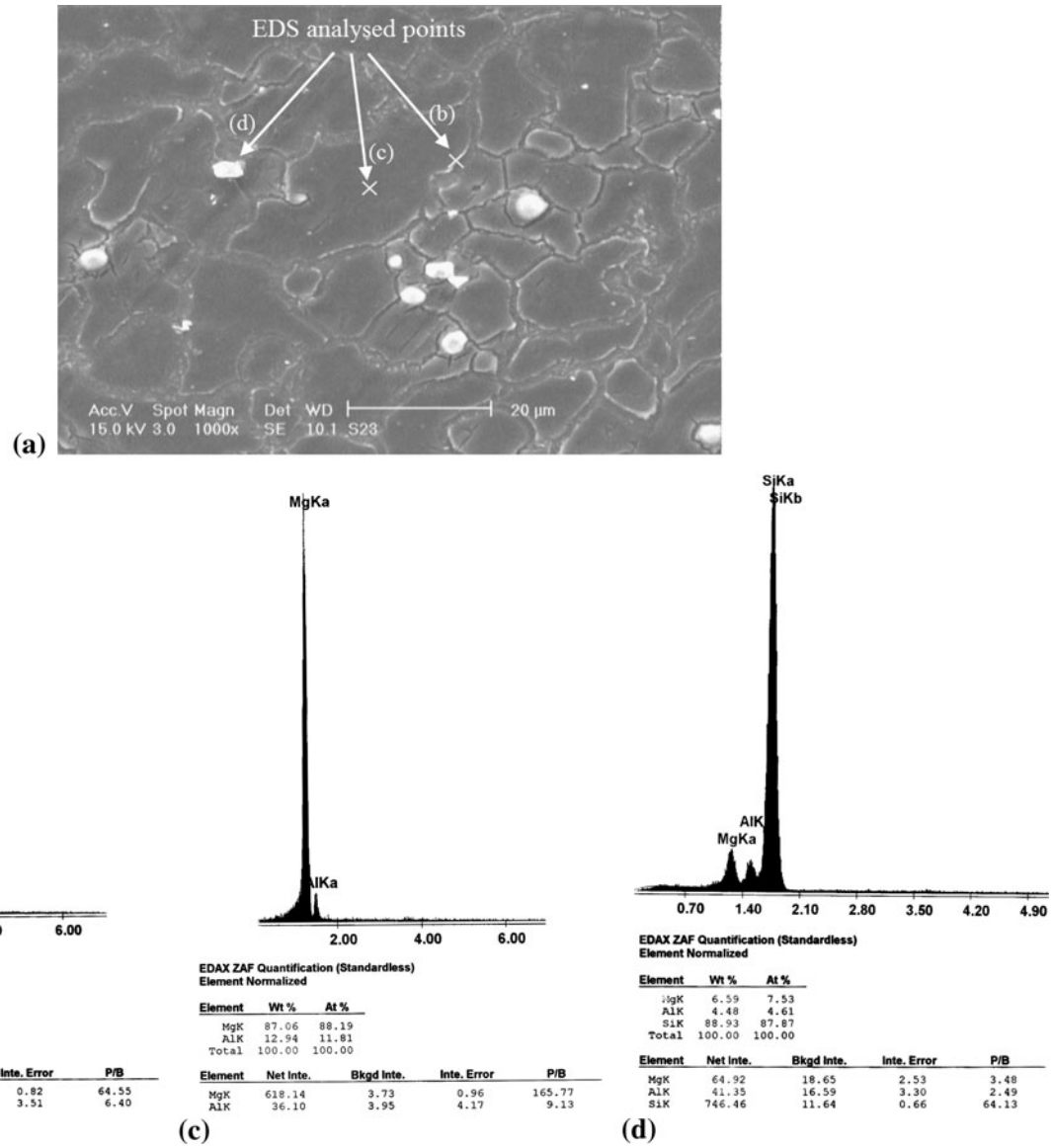

Fig. 3 (a) SEM micrograph of SZ, EDS results (b) near the grain boundary, (c) inside the grain, and (d) on the white particles in (a). The specimen FSPed with 5 µm SiC particles. The rotational and traverse speeds were 900 rpm and 63 mm/min, respectively

presence of SiC particles. Consequently, it can be inferred that SiC particles exhibit effective interaction with grain boundaries.

3.1 Effect of Rotational Speed and SiC Particle Size on Microstructure and Microhardness

Figure 4 shows the microstructure of FSPed specimen without SiC particles at different rotational speeds. Decreasing rotational speed resulted in grain size reduction. The phenomenon which forces thermomechanically processed materials to have very small grains is called dynamic recrystallization.

This phenomenon is classified into continuous and discontinuous recrystallizations. During the process, material undergoes severe plastic deformation; as a result, a large number of low-angle misorientated grain boundaries are created. In general, the recovery process of these grains and conversion of low angle boundaries to high angle ones are considered as continuous dynamic recrystallization (CDRX). The nucleation of new grains at preferential sites such as pre-existing grain boundaries and the places with high stored energy takes place as a result of discontinuous dynamic recrystallization (DDRX) (Ref 15, 16). Approaching the lowest level of energy by decreasing the grain boundaries surfaces, the new fine grains start growing, if enough time and heat are provided. The higher the rotational speed, the more the heat generation, and the faster the grain growth, especially in the lack of SiC particles.

Figure 5 shows effects of the rotational speed on grain size and hardness of the SZ with the additions of various SiC particles. It can be concluded from Fig. 5(a) that addition of SiC particles fades the effect of generated heat on the grain growth as the rotational speed increases. Also, the rotational speed has no significant effect on the grain size of the specimen with 30 nm SiC particles.

During deformation, regardless of SiC particles, grains break into smaller sizes. Therefore, a large number of high angle grain boundaries are produced (Ref 15). However, in this

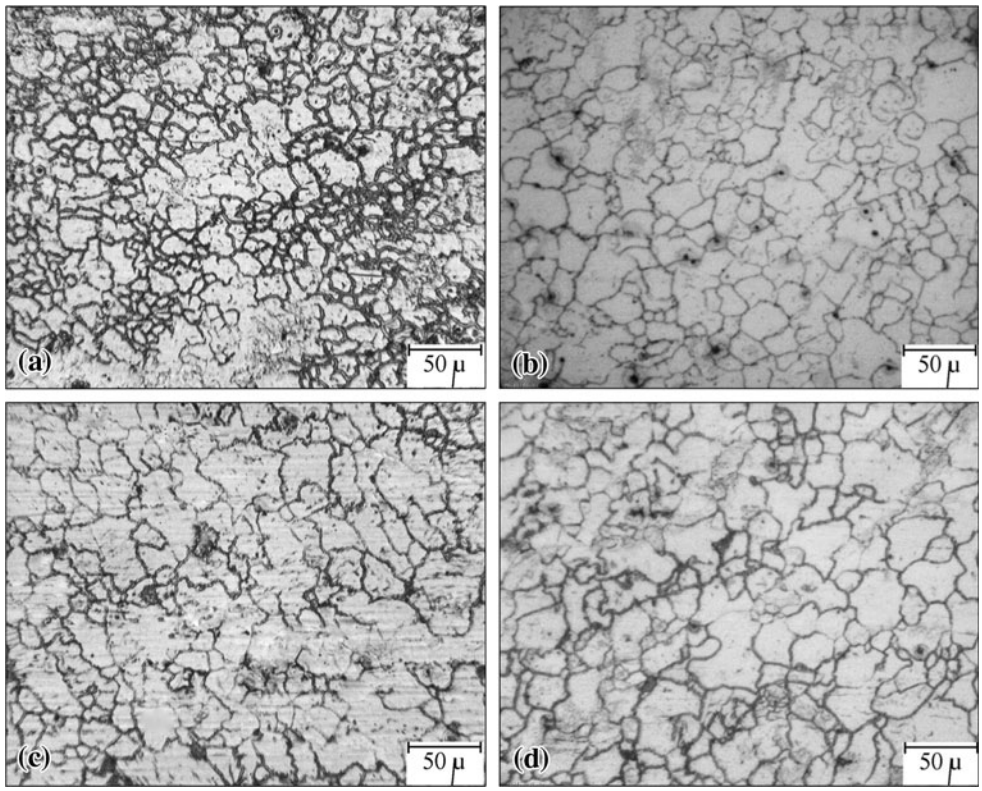

Fig. 4 Microstructure of FSPed sample without SiC particles at the rotational speed of (a) 710 rpm, (b) 900 rpm, (c) 1120 rpm, and (d) 1400 rpm. The traverse speed was 12.5 mm/min

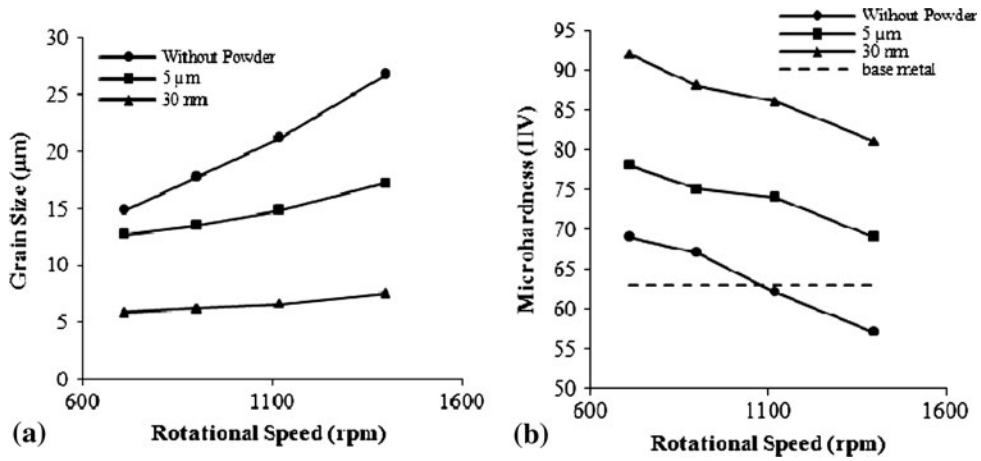

Fig. 5 Effect of the rotational speed on (a) grain size of SZ, and (b) microhardness of SZ; in the samples FSPed with and without 5 μm and 30 nm SiC particles. The traverse speed was 12.5 mm/min

case, addition of SiC particles leads to inhomogeneous local deformation that assists the break-up of the grains. According to Fig. 5(a), it seems that this phenomenon is highly affected by the number and size of SiC particles. While the grain size of the specimens with and without 5 μm SiC particles is rather close, there is a huge difference in the cases of specimens with nano particles. The number of 30 nm SiC particles is much more than 5 μm ones. Consequently, the effect of grain breaking is more intensive.

Grain growth is another major parameter that should be noticed. According to the Zener limiting grain size principle, assuming a completely uniform distribution of clustering nano-sized SiC particles, the Zener limiting grain size (d_z) can be calculated by $d_z = 4r/(3V_f)$, where r and V_f are the radius and volume fraction of clustering SiC particles, respectively. It is clear that decreasing the particles' radius increases the pinning effect of them (Ref 17-19). According to this principle, there are two major factors determining the final grain size after

recrystallization: the radius and volume fraction of particles. The smaller particle size causes higher restriction to grain growth.

Consequently, the presence of nano particles leads to considerably fine grain size because of more breakage of primary grains, excellent pinning of grain boundaries and more grain nucleation sites. It is worthy to say that the residual stress around particles resulted from the difference between thermal expansion coefficients of matrix and that particles stimulate the recrystallization and leads to smaller grain size (Ref 20).

In addition, the difference between the grain sizes of the samples with and without 5 μm SiC particles decreases as the rotational speed falls down. Therefore, at the lower rotational speeds, the effect of 5 μm particles in grain refinement is not considerable because the generated heat and consequently the grain growth are not so intense and also the amount of grain breakage by these particles is negligible.

As shown in Fig. 5(b), the higher the rotational speed, the higher the grain size, and the less the microhardness. The Hall-Petch relation expresses that the hardness has an inverse correlation with the grain size (Ref 21). But, there is an exception: the SZ hardness of sample FSPed without SiC particles at the rotational speed of 1400 rpm was less than that of the base metal (63 HV), despite the decrease in the grain size (from ~150 to ~27 μm). It was the result of dissolution of strengthening β ($Mg_{17}Al_{12}$) phase during the FSP which was previously discussed (Fig. 3).

Additionally, Fig. 5(b) shows that the microhardness of samples FSPed in the same conditions increases by adding SiC particles due to their own hardness and Orowan mechanism. This mechanism explains the interaction of dislocations with the non-shearable SiC particles. According to this mechanism, dislocations make loops and bypass the particles. In fact, the particles act like a barrier in front of the dislocation movement

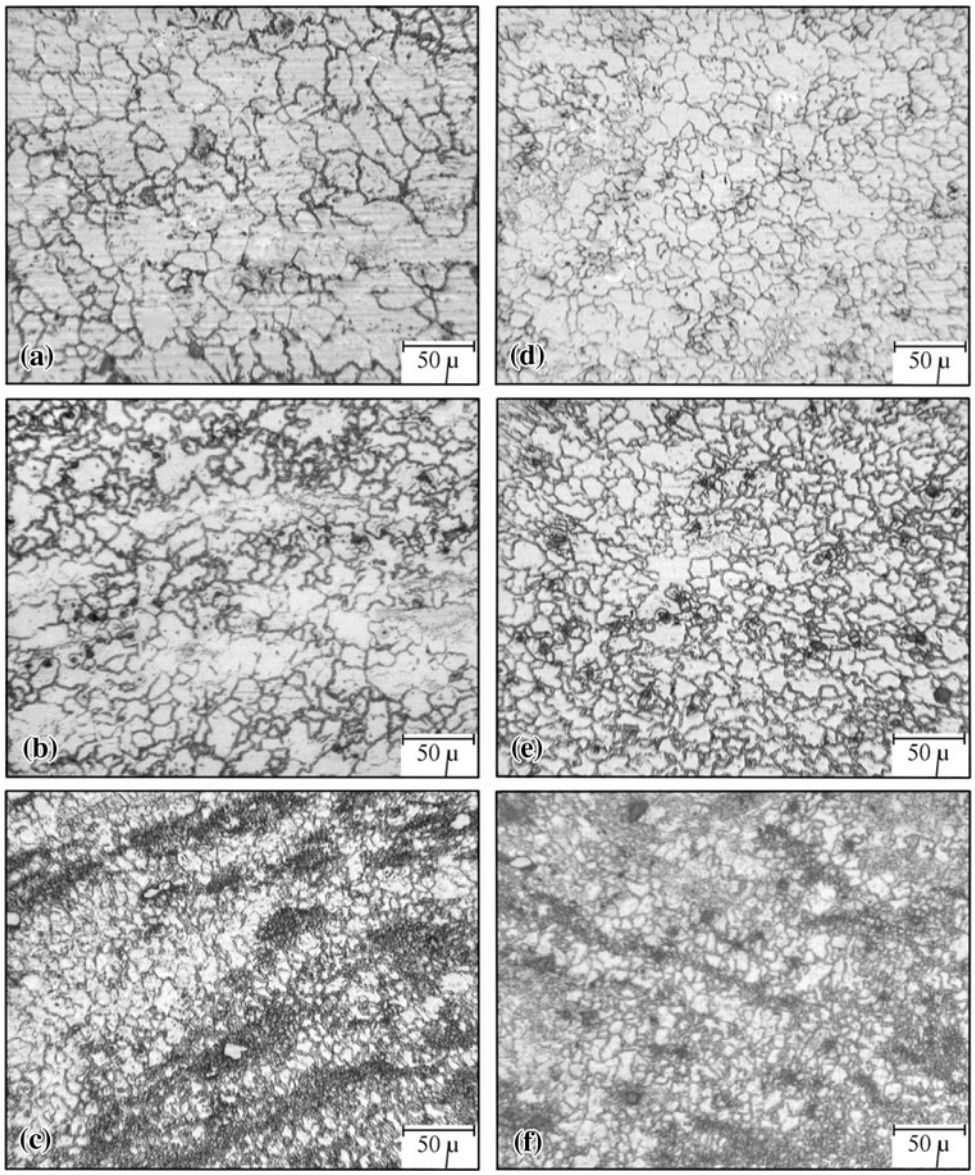

Fig. 6 Microstructure of FSPed samples (a) and (d) without SiC particles, (b) and (e) with 5 μm SiC particles, (c) and (f) with 30 nm SiC particles. Traverse speed: (a)-(c) 12.5 mm/min, and (d)-(f) 63 mm/min. Rotational speed: 1120 rpm

and lead to increase in strength and hardness of the composite samples. $\Delta\sigma_{Orowan}$ can be calculated as follows (Ref 4, 22):

$$\Delta\sigma_{Orowan} = \frac{KG_m b}{\lambda} \ln \frac{d_p}{2b}$$

where b is the Burgers vector, d_p is the average diameter of particles, G_m is the shear modulus of matrix, λ is the inter-particle spacing, and K is a constant determined by experiment.

Beside grain size and reinforcing particles as major factors, work hardening due to the strain misfit between the elastic reinforcing particles and plastic matrix, and thermal strains caused by different expansion coefficients of particles and matrix, also increase the hardness of SZ.

From Fig. 5(b) it could be inferred that the average microhardness of the nanocomposite layer FSPed at the rotational and traverse speeds of 710 rpm and 12.5 mm/min respectively, reached 92 HV which means ~46% rise as compared to the base metal.

3.2 Effect of Traverse Speed and SiC Particle Size on Microstructure and Microhardness

Microstructures of FSPed specimens with and without 5 μm and 30 nm SiC particles at two distinct traverse speeds are shown in Fig. 6. The grain sizes of these specimens are shown in Table 1. The grain size of the specimens without particles is the largest with respect to the specimens with nano-sized SiC particles which is the lowest in both traverse speeds. The powder distribution and microstructure of the specimen with

Table 1 Effects of the SiC particle size and the traverse speed on the grain size of SZ

	Grain size, μm		
	Traverse speed 12.5 mm/min	Traverse speed 63 mm/min	$GS_{12.5} - GS_{63}$
Without SiC particles	21.16	10.12	11.04
5 μm	14.82	9.52	5.3
30 nm	6.58	5.21	1.37
$GS_{without} - GS_{5\ \mu m}$	6.34	0.6	
$GS_{5\ \mu m} - GS_{30\ nm}$	8.24	4.31	

The rotational speed was 1120 rpm

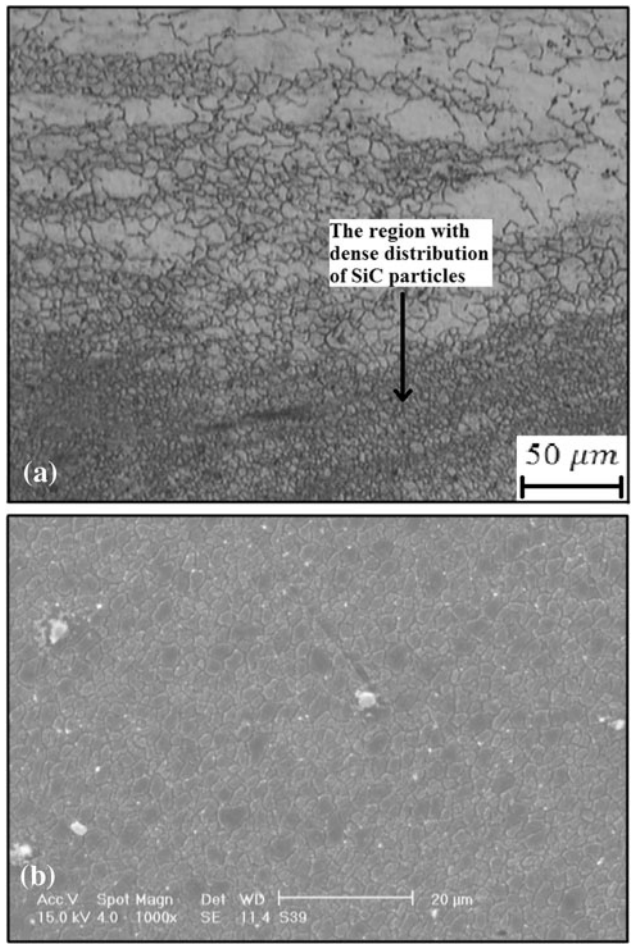

Fig. 8 (a) Non-uniform distribution of nano-sized SiC particles in magnesium matrix, (b) SEM image of the region with dense distribution of nano-sized SiC particles. The rotational and traverse speeds were 1120 rpm and 40 mm/min, respectively

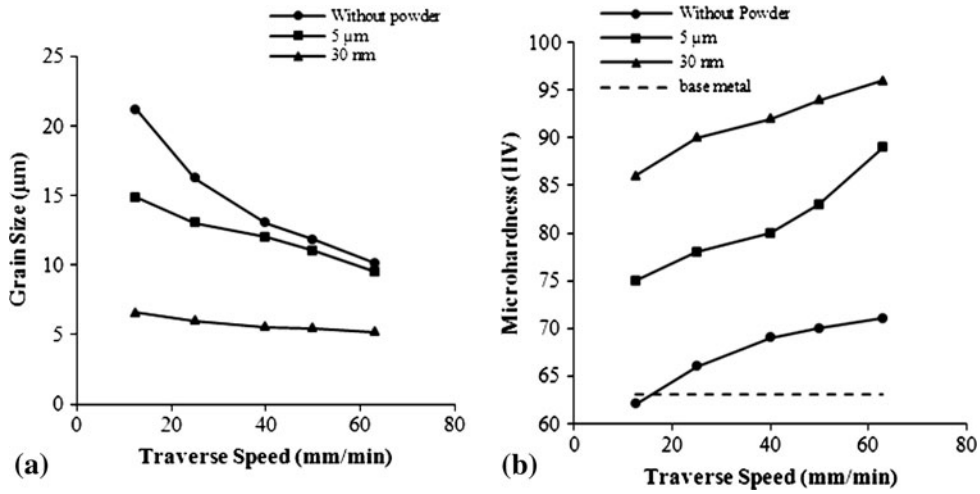

Fig. 7 Effect of the traverse speed on the (a) grain size of SZ, and (b) microhardness of SZ in several SiC particle sizes. The rotational speed was 1120 rpm

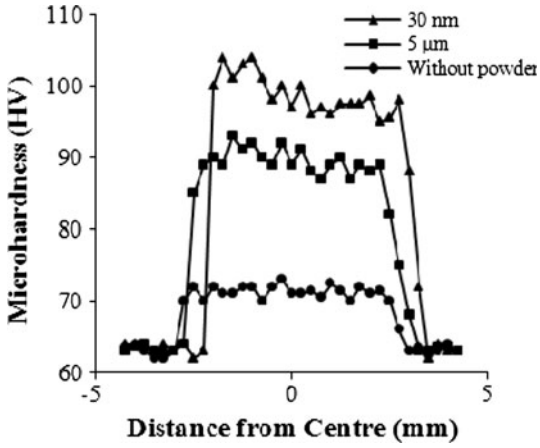

Fig. 9 Microhardness profile of the FSPed samples with and without 5 μm and 30 nm SiC particles. The rotational and traverse speeds were 1120 rpm and 63 mm/min, respectively

nano-sized SiC particles is almost non-uniform. Figure 7 shows the effects of the traverse speed and SiC particles on grain size and hardness of SZ. Two interesting results are observed in Fig. 7(a) and Table 1. First, the difference of grain sizes between the specimens with and without 5 μm and 30 nm SiC particles becomes larger as the traverse speed decreases. This confirms the results obtained by Morisada et al. (Ref 1). Second, the grain size of the specimen without particles in traverse speed of 63 mm/min is smaller than that of the specimen with 5 μm particles in traverse speed of 50 mm/min. It should be noted that these two phenomena are similar to effects of rotational speed and the presence of particles that were discussed in detail in section 3.1.

3.3 Effect of FSP Pass Number and SiC Particle Size on Microstructure and Microhardness

As is clear from Fig. 8(a), nano-sized SiC particles were not distributed uniformly in the matrix during the stirring process

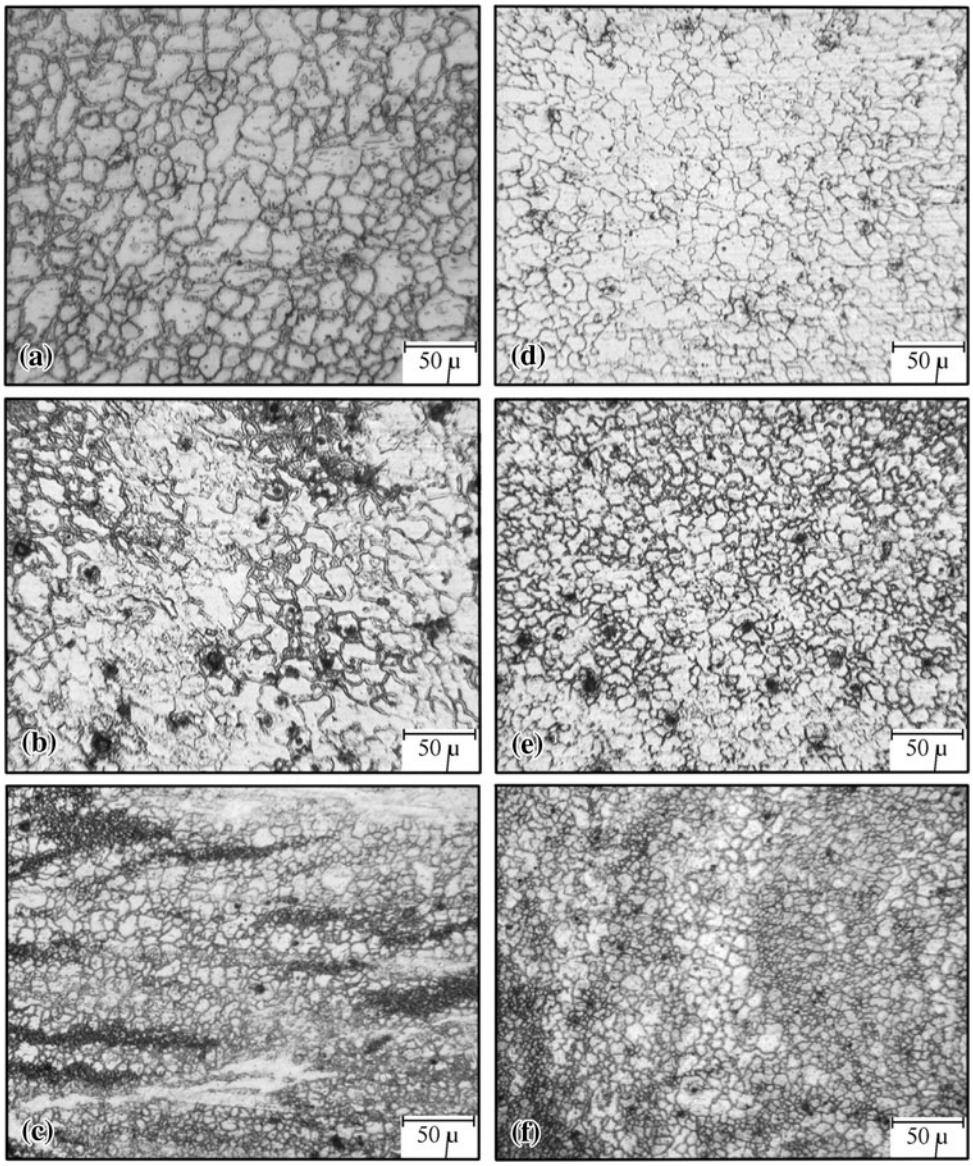

Fig. 10 Microstructure of the specimen (a), (d) without particles, (b), (e) with 5 μm particles, (c), (f) with 30 nm particles. (a)-(c) Produced by one FSP pass, (d)-(f) produced by two FSP passes. The rotational and traverse speeds were respectively 1120 rpm and 50 mm/min in both FSP passes

because the particles agglomerated particularly in single pass FSP. The darker regions pointed in Fig. 8(a) have dense distribution of reinforcing particles. Because of such non-uniformity, the grain size distribution also became non-uniform after recrystallization. The higher density of the particles in certain areas prevented grain growth during recrystallization; therefore, the grain size in these regions became even finer than 2 μm (Fig. 8b).

The hardness profile of the SZ is found to be influenced by the powder size and the grain size in different locations. Figure 9 shows the hardness profile in the specimens with and without 5 μm and 30 nm SiC particles. The average hardness of the specimen with nano-sized particles is the highest value (96 HV), whereas the lowest hardness belongs to the specimen without reinforcing particles (71 HV). However, the hardness profile of the specimen without particles is smoother than those of the two other specimens with SiC particles.

The effect of FSP pass number on microstructure of the specimens with and without 5 μm and 30 nm SiC particles is shown in Fig. 10. The grain sizes of these samples are shown in Table 2. The microstructure of samples refined due to dynamic recrystallization of the second FSP pass. It is inferred from Table 2 that the grain size reduction by second FSP pass in the samples with nano-sized SiC particles is the highest value (45%), whereas it is the lowest for the specimen without SiC particles (7%). However, it should be mentioned that the second FSP pass does not always decrease the grain size. For instance, Fig. 11 shows an increase in grain size after second FSP pass at the rotational and traverse speeds of 1120 rpm and 12.5 mm/min, respectively. The specimens without SiC particles at lower traverse and higher rotational speeds show an increase in grain size because of overheating during the second pass.

Table 2 Effects of FSP pass number and reinforcing particle sizes on the grain size of SZ

	Grain size, μm			
	1 pass FSP	2 pass FSP	$GS_{1\ pass} - GS_{2\ pass}$, μm	ΔGS, %
Without particle	11.8	10.94	0.86	7.3
5 μm	11.02	7.7	3.32	30.1
30 nm	5.46	3	1.75	45

The rotational and traverse speeds were 1120 rpm and 50 mm/min, respectively

Figure 12 shows the hardness profile of the specimens produced by one and two FSP passes with 30 nm SiC particles. As could be seen, the average hardness in the stirred zone was increased from 94 to 107 HV by the second FSP pass, due to the decrease of grain size.

It is noteworthy to say that, the same as grain size, the hardness of the specimen without SiC particles was not affected significantly by the second FSP pass (for the same parameters cited in Fig. 12). On the other hand, for the specimen produced by two FSP passes without SiC particles at the rotational and traverse speeds of 1120 rpm and 12.5 mm/min respectively, the hardness of SZ decreased from 62 to 54 HV. This means that the second FSP pass at higher rotational and lower traverse speeds decreases the hardness of specimens without SiC particles due to the grain growth.

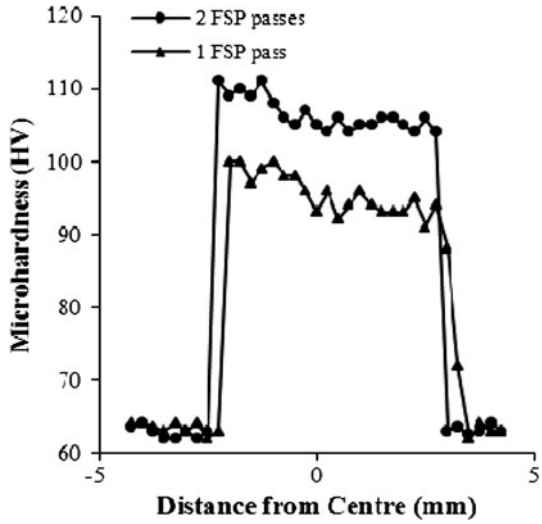

Fig. 12 Microhardness profile of the specimens produced by one and two FSP passes with 30 nm SiC particles. The rotational and traverse speeds were 1120 rpm and 50 mm/min, respectively

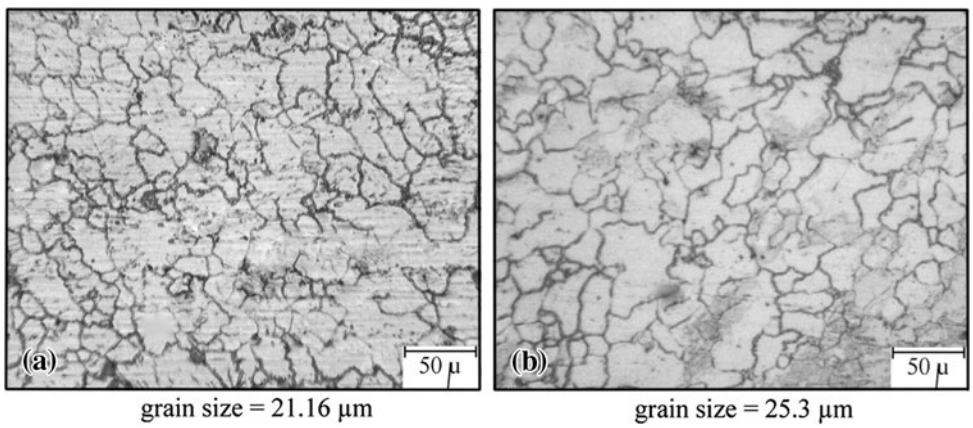

Fig. 11 Microstructure of specimen produced by (a) one FSP pass, (b) two FSP passes, and without SiC particles. The rotational and traverse speeds were 1120 rpm and 12.5 mm/min, respectively

4. Conclusions

In this investigation, friction stir processing (FSP) as a modification process was carried out on the as-cast AZ91 magnesium alloy and AZ91/SiC composite and nanocomposite layer was successfully fabricated on its surface. Effect of the process parameters and reinforcing particles size on the microstructure and hardness of the fabricated surface was investigated. Results showed the following:

1. A homogenous microstructure with a uniform chemical composition was developed by FSP due to dissolution of eutectic β-phase precipitated near the grain boundaries.
2. The effect of nano-sized SiC particles on the grain size and hardness of the fabricated layer is found to be more impressive than micro-sized particles. Incorporation of nano-sized SiC particles into AZ91 magnesium matrix decreases the grain size severely (from ~150 to ~5 μm) and increases the microhardness to a considerable degree as well (from 63 to 96 HV).
3. Increasing the rotational speed increases the grain size as the hardness decreases. The grain growth rate of the specimen FSPed without SiC particles is high while employing SiC particles, especially nano-sized particles, restricting the grain growth severely.
4. The effect of the traverse speed on the grain size and the hardness is opposite to that of the rotational speed.
5. Second FSP pass increases the hardness and decreases the grain size of the specimens FSPed with SiC particles and enhances distribution of SiC particles. However, it does not have any significant effect on the grain size and hardness of FSPed specimens without particles.

Acknowledgment

Iranian Nanotechnology Initiative is gratefully appreciated for partial financial support.

References

1. Y. Morisada, H. Fujii, T. Nagaoka, and M. Fukusumi, Effect of Friction Stir Processing with SiC Particles on Microstructure and Hardness of AZ31, *Mater. Sci. Eng. A*, 2006, **433**, p 50–54
2. C.I. Chang, X.H. Dua, and J.C. Huang, Achieving Ultrafine Grain Size in Mg-Al-Zn Alloy by Friction Stir Processing, *Scripta Mater.*, 2007, **57**, p 209–212
3. P. Cavaliere and P.P. De Marco, Superplastic Behaviour of Friction Stir Processed AZ91 Magnesium Alloy Produced by High Pressure Die Cast, *J. Mater. Process. Technol.*, 2007, **184**, p 77–83
4. M. Habibnejad-Korayem, R. Mahmudi, and W.J. Poole, Enhanced Properties of Mg-Based Nano-Composites Reinforced with Al_2O_3 Nano-Particles, *Mater. Sci. Eng. A*, 2009, **519**, p 198–203
5. C.J. Lee, J.C. Huang, and P.L. Hsieh, Using Friction Stir Processing to Fabricate Mg Based Composites with Nano Fillers, *Key Eng. Mater.*, 2006, **313**, p 69–74
6. C.J. Hsu, P.W. Kao, and N.J. Ho, Ultrafine-Grained Al-Al_2Cu Composite Produced In Situ by Friction Stir Processing, *Scripta Mater.*, 2005, **53**, p 341–345
7. S.F. Hassan and M. Gupta, Development of High Performance Magnesium Nano-Composites Using Nano-Al_2O_3 as Reinforcement, *Mater. Sci. Eng. A*, 2005, **392**, p 163–168
8. G. Cao, H. Choi, J. Oportus, H. Konishi, and X. Li, Study on Tensile Properties and Microstructure of Cast AZ91D/AlN Nanocomposites, *Mater. Sci. Eng. A*, 2008, **494**, p 127–131
9. C.J. Lee, J.C. Huang, and P.J. Hsieh, Mg Based Nano-Composites Fabricated by Friction Stir Processing, *Scripta Mater.*, 2006, **54**, p 1415–1420
10. Y. Morisada, H. Fujii, T. Nagaoka, and M. Fukusumi, MWCNTs/AZ31 Surface Composites Fabricated by Friction Stir Processing, *Mater. Sci. Eng. A*, 2006, **419**, p 344–348
11. Y. Morisada, H. Fujii, T. Nagaoka, K. Nogi, and M. Fukusumi, Fullerene/A5083 Composites Fabricated by Material Flow During Friction Stir Processing, *Composites Part A*, 2007, **38**, p 2097–2101
12. P. Asadi, G. Faraji, and M.K. Besharati, Producing of AZ91/SiC Composite by Friction Stir Processing (FSP), *Int. J Adv. Manuf. Technol.*, 2010, **51**, p 247–260
13. L. Cizek, M. Gregera, L. Pawlicaa, L.A. Dobrzanskib, and T. Tanskib, Study of Selected Properties of Magnesium Alloy AZ91 After Heat Treatment and Forming, *J. Mater. Process. Technol.*, 2004, **157–158**, p 466–471
14. P. Cavaliere and P.P. De Marco, Friction Stir Processing of AM60B Magnesium Alloy Sheets, *Mater. Sci. Eng. A*, 2007, **462**, p 393–397
15. F.J. Humphreys, P.B. Prangnell, and R. Priestner, Fine-Grained Alloys by Thermomechanical Processing, *Curr. Opin. Solid State Mater. Sci.*, 2001, **5**, p 15–21
16. S.M. Fatemi-Varzaneh, A. Zarei-Hanzaki, and H. Beladi, Dynamic Recrystallization in AZ31 Magnesium Alloy, *Mater. Sci. Eng. A*, 2007, **456**, p 52–57
17. A. Shafiei-Zarghani, S.F. Kashani-Bozorg, and A. Zarei-Hanzaki, Microstructures and Mechanical Properties of Al/Al_2O_3 Surface Nano-Composite Layer Produced by Friction Stir Processing, *Mater. Sci. Eng. A*, 2009, **500**, p 84–91
18. R.S. Mishra and Z.Y. Ma, Friction Stir Welding and Processing, *Mater. Sci. Eng. R*, 2005, **50**, p 1–78
19. R.E. Reed-Hill and R. Abbaschian, *Physical Metallurgy Principles*, 3rd ed., PWS Publishing Company, 1994, p 315–318
20. I. Toda-caraballo, J. Chao, L.E. lindgren, and C. Capdevila, Effect of Residual Stress on Recrystallization Behavior of Mechanically Alloyed Steels, *Scripta Mater.*, 2010, **62**, p 41–44
21. B.M. Darras, M.K. Khraisheh, F.K. Abu-Farha, and M.A. Omar, Friction Stir Processing of Commercial AZ31 Magnesium Alloy, *Mater. Process. Technol.*, 2007, **191**, p 77–81
22. X.L. Zhong, W.L.E. Wong, and M. Gupta, Enhancing Strength and Ductility of Magnesium by Integrating it with Aluminum Nanoparticles, *Acta Mater.*, 2007, **55**, p 6338–6344